



Atomic force microscope observation of athletes' hemoglobin imaging

Guojun Zhang^{1*}, Weidong Luo¹, Shereen Ismail Hajee², HanCheng Gong³

¹ College of Physical Education, Northwest Normal University, Lanzhou 730070, China

² Lecturer, Biophysics Unit, Departement of Basic Science, College of Medicine, Hewler Medical University, Kurdistan Region-Iraq

³ College of Letters & Science, University of California Santa Barbara, Santa Barbara 93106, United States of America

*Correspondence to: xbsdzgi@163.com

Received March 5, 2020; Accepted August-15-2020; Published October 31, 2020

Doi: <http://dx.doi.org/10.14715/cmb/2020.66.7.14>

Copyright: © 2020 by the C.M.B. Association. All rights reserved.

Abstract: Hemoglobin (Hb) is a protein and its functional form has a tetrameric structure. This structure is the result of a combination of four sub-units called globin and indicates the dynamic interaction between them. Each subunit has a ring-shaped organic molecule called a heme that contains an iron atom; Heme is a group that mediates the reversible binding of oxygen by hemoglobin. This research was performed to observe the image of Hb by an atomic force microscope (AFM) and measure the physical function of athletes. For this purpose, based on the principle of AFM imaging, the hemoglobin crosslinking method was used to measure the morphology and size of cross-linked Hb, glutaraldehyde and Hb diameter were detected to prepare cross-linked Hb samples with different molar ratio, the activity of peroxidase was detected by Trinder reaction. The AFM was used to detect the influence of physiological environment changes such as pH, temperature, oxygen partial pressure and osmotic pressure on the absorption spectrum of Hb imaging. Results showed that the size of the uncrosslinked Hb was 6.64 nm. With the increase of the molar ratio of glutaraldehyde to Hb, the number of Hb molecules involved in the crosslinking increased, and the molecular size increased. During the crosslinking process, the aggregation of the cross-linked molecules would make the particle size of some Hb molecules reach 80-100 nm. The peak height, peak position and peak shape of the characteristic absorption peaks of pH to hemoglobin at 550 and 589 nm occurred. When the temperature changes continuously in the range of 30-55°C, the peak height of Hb absorption spectrum of normal red blood cells at 550 nm and 589 nm decreases gradually with the increase of temperature, and the peak shape at 610 nm changes obviously at 42°C, which indicates that the molecular structure of Hb changes; the absorption spectrum curve of deoxygenation disappears at 500 nm, the oxygen-binding capacity of Hb is very low, and the oxygen affinity and oxygenated hemoglobin are low (The concentration of HbO₂) decreased, the osmotic pressure increased, the RBC dehydrated, the volume decreased, and the concentration of Hb increased. Conclusion: It is more accurate and comprehensive to use AFM to observe athletes' hemoglobin.

Key words: Microscope; Hemoglobin; Body Function; Imaging; Environment; pH.

Introduction

The physiological advantage of the presence of hemoglobin (Hb) in red blood cells is the improvement in oxygen delivery to tissues and organs. The solubility of oxygen in water is very low, so small amounts of oxygen are transported through diffusion. Hb allows oxygen to be transported more rapidly and efficiently than diffusion. Hb is a protein found in red blood cells that plays a key role in carrying oxygen and carbon dioxide. In the current scientific training, coaches need to evaluate the training effect of athletes by understanding their physical skill level. Hb can be used as a biochemical index for coaches to evaluate the physical function, nutritional status and exercise load of athletes. Hemoglobin (Hb), relative molecular weight 65500da, commonly known as hemoglobin, is an oligomeric protein composed of four peptide chains by a covalent bond. It is the main component of red blood cells, accounting for about 95% of the dry weight of red blood cells. The main physiological function of hemoglobin is to transport oxygen and carbon dioxide, participate in the regulation of acid-base balance in the body (1), so it directly affects the metabolism of substance and energy in the

body, thus affecting the body function and exercise ability. Therefore, the research on hemoglobin imaging of athletes' body function has attracted the attention of scientists (2-4). Atomic force microscopy (AFM) can be used to measure the shape characteristics of micro-objects by using the force relationship between atoms. Because of its high vertical and horizontal resolution and non-destructive testing method, it is recognized as an ideal ultra-smooth surface morphology analyzer. The research of AFM, which covers all aspects of industrial production, microelectronics, micro detection, nanotechnology and biotechnology, has a wide range of application prospects in physics, chemistry, medicine, materials science and microelectronics. In this paper, the imaging of athletes' body functional hemoglobin is observed by atomic force microscope, which overcomes the traditional micro-spectrophotometric system's long detection time due to the single-channel optical detection, which is difficult to carry out the spectral detection of time resolution requirements and multi-component material analysis (5, 6). Endurance exercise can lead to the abnormal metabolism of free radicals in the body, resulting in protein cross-linking. Therefore, it is more effective to detect the cross-linking hemoglobin of dif-

ferent athletes under the change of physiological environment when testing the hemoglobin of athletes' body function. AFM technology can detect the spectrum of micro samples in the wavelength range of 350-800 nm (the shortest detection time is 1 ms), and the wavelength resolution is 0.2 nm. AFM technology has the characteristics of high resolution, adjustable integration time, high signal-to-noise ratio, small volume and easy operation. In addition to the optical density measurement, spectral absorption measurement and fluorescence measurement of biological tissues, cells, cell products, bacteria and parasites, the dynamic study of the changes of the molecules in a single living cell with physiological and biochemical conditions can be carried out (7), the detection of apoptosis process, the monitoring of cell discharge (secretion) during the opening and closing of cell ion channels, and the monitoring of single living cells with multi-molecular probes Cell fluorescence detection and spectral analysis of micro rapid biological events (8-11).

Through the measurement of hemoglobin size, the activity of cross-linked hemoglobin peroxide and the physiological environment inside and outside the cells of athletes' body function hemoglobin, it is found that the size of hemoglobin is similar to that of X-ray diffraction PH, temperature, oxygen partial pressure, osmotic pressure and the concentration of 2,3-DPG in red blood cells are important factors affecting the structure and function of Hb. In this paper, using AFM technology, combined with the use of microcell culture cell to change the physiological environment of cells (pH, temperature, oxygen partial pressure, osmotic pressure), the continuous and rapid monitoring of the absorption spectrum of HB molecules has been realized (12).

Materials and Methods

Experiment principle

According to the basic structure of the AFM system, when the light source of the inverted microscope irradiates the sample through the focused probe-type composite beam, the sample is selectively absorbed. According to Lambert-Beer law, the transmittance in the range of the incident wavelength is:

$$Q = \frac{\int_{\gamma_a}^{\gamma_b} B\gamma I\gamma^{-A\gamma} d\gamma}{\int_{\gamma_a}^{\gamma_b} B\gamma I\gamma d\gamma} \quad \{1\}$$

Where, $B\gamma$ is the relative sensitivity of detection, $I\gamma$ is the intensity of incident light, $I\gamma \cdot 10^{-A\gamma}$ is the intensity of transmitted light, and γ at γ_a to γ_b is the spectral width. In the spectrometer, the composite transmission spectrum is uniformly expanded on n image sensitive units of the linear array multichannel detector. Because the spectral width $d\gamma = (\gamma_b - \gamma_a) / n$ received by a single pixel is small enough, $d\gamma$ is the monochromatic absorption layer at the corresponding position of the spectrum, and its absorbance $A\gamma$ is:

$$A\gamma = \log \frac{I_{\gamma_0}}{I_{\gamma_i}} = \kappa_{\gamma} \cdot c \cdot l \quad \{2\}$$

is the thickness of the absorption layer, κ_{γ} is the molar absorption coefficient, and C is the molar concentration of the sample. For a multi-component absorption system, the absorbance is additive. If there are n com-

ponents, the total absorbance at a certain wavelength in the detection spectrum is:

$$A(\gamma) = \sum_{i=1}^n \kappa_i \gamma \cdot c_i \cdot l \quad \{3\}$$

The concentration of n components in the system can be determined by solving n linear equations. Because the CCD spectral detector has a certain dark current output $I_d(\gamma)$, the actual absorbance is:

$$A(\gamma) = \log \frac{I_s(\gamma) - I_d(\gamma)}{I_i(\gamma) - I_d(\gamma)} \quad \{4\}$$

$I_s(\gamma)$ is the transmitted light intensity of the sample, and $I_i(\gamma)$ is the transmitted light intensity of the sample generation environment. The optical signal is amplified and sent to the A/D synchronous data acquisition card. The acquisition is controlled by the synchronous signal sent by the CCD, which ensures that the A/D conversion time is always at the flattest part of the CCD output signal, so the collected data is relatively stable. The system computer reads the A/D conversion data stored in the acquisition card one by one through the ISA bus and processes the real-time digital signal according to a different analysis and calculation methods It can be used for rapid analysis of various micro samples.

Experimental method

Crosslinking of hemoglobin

Preparation of phosphoric acid buffer solution

0.1 mol/L Na_2HPO_4 solution and 0.1 mol/L KH_2PO_4 solution were put into pH 5.6 phosphoric acid buffer solution for standby.

Preparation of hemoglobin solution and glutaraldehyde (GTA) solution

Take 100 mL of the above prepared phosphoric acid buffer solution with pH 5.6, weigh 0.0813 gHb to prepare 100 mL of the solution, that is, 1.25×10^{-5} mol/L hemoglobin solution; the glutaraldehyde concentration used in the laboratory is 0.25 g/mL, after four dilutions, prepare 100 mL of 2.5×10^{-4} mol/L solution.

Crosslinking treatment of hemoglobin

Take 25 mL of hemoglobin solution prepared above

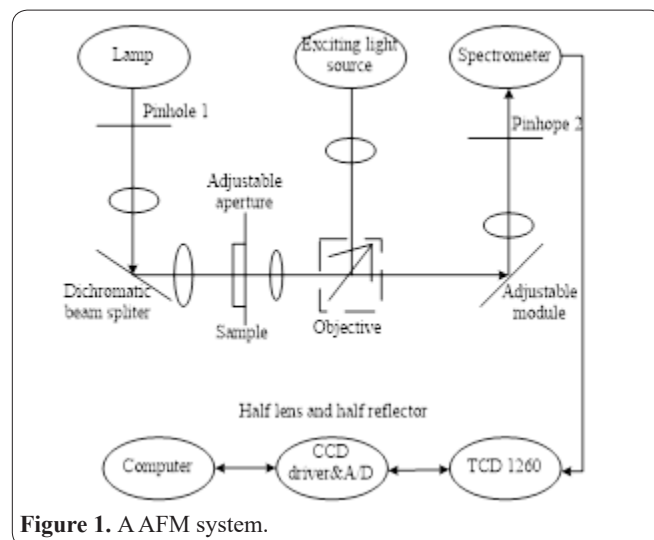


Figure 1. A AFM system.

and put them into beakers A, B, C and D respectively, add 1.25 mL, 6.25 mL, 12.5 mL and 25 mL of glutaraldehyde respectively, so that the molar ratio of glutaraldehyde to hemoglobin is 1:1, 5:1, 10:1 and 20:1 respectively. Glutaraldehydecross-linked hemoglobin was prepared by magnetic stirring for 2 hours.

Observation of hemoglobin morphology

The glutaraldehyde cross-linked hemoglobin solution prepared above was used to prepare samples, and the size and morphology of hemoglobin were observed by AFM.

Hemoglobin cross-linked hemoglobin peroxidase activity determination

Calibration of hydrogen peroxide concentration

Preparation of potassium permanganate solution

Weigh about 1.6 g of KMnO_4 into the beaker, add 500 mL of water, cover the watch glass, heat it to boiling, keep it slightly boiling for 1h, filter it with glass sand core funnel after cooling to remove MnO_2 impurities, and then store the solution in 500 mL brown bottle, which can be directly used for calibration.

Calibration of potassium permanganate solution

Weigh a certain amount of $\text{Na}_2\text{C}_2\text{O}_4$ into a conical flask, add 40 mL of water, then add 10 mL, 3 mol/L of H_2SO_4 solution (12 mL of sulfuric acid + 63 mL of water, namely $\rho_{\text{H}_2\text{SO}_4}=1.84$ g/mL), heat to 75-85°C (the temperature when the steam starts to flow), and titrate with KMnO_4 solution to be calibrated when it is hot. Then the concentration of potassium permanganate is:

$$C_{\text{KMnO}_4} = \frac{m_{\text{Na}_2\text{C}_2\text{O}_4} \times 2}{134 \times V_{(\text{KMnO}_4)} \times 5} \quad \{5\}$$

Determination of H_2O_2 content in dioxygen water

Pipette 1.00 mL of hydrogen peroxide into a 250 mL volumetric flask, add water to dilute and set the scale, shake it well, pipette 20.00 mL into a 250 mL conical flask, add 2-3 drops of 1 mol/L MnSO_4 solution of 3mol/L of H_2SO_4 phase, titrate it with KMnO_4 standard solution until it is reddish, do not fade within half a minute as the titration endpoint, and conduct parallel determination for three times. Then the content of H_2O_2 is:

$$\rho(\text{H}_2\text{O}_2) / (\text{g}/100\text{ml}) = \frac{(cV)\text{KMnO}_4 \times 5 \times 34.02 \times 100}{1000 \times 1.00 \times 2 \times 20.00 / 250.00} \quad \{6\}$$

$\rho(\text{H}_2\text{O}_2)$ was used in laboratory = 33.16g/100mL = 9.75 mol/L

Preparation of H_2O_2 solution

Measure 3.83 mL H_2O_2 ($\rho = 33.16/100\text{mL}$) in a 250 mL volumetric flask with a pipette, add distilled water to the scale, and then 0.15M H_2O_2 solution is obtained.

Determination of pH, temperature, oxygen partial pressure and osmotic pressure

Blood samples were taken from the vein blood of healthy people confirmed by physical examination. The

sample is placed in a special micro cell sample cell designed by ourselves. The cell sample cell combines with thermostat, constant temperature circulating water supply, constant gas circulation supply and pipette dosing pump device to achieve the functions of cell sample maintenance, constant temperature, constant gas content and culture medium perfusion. During the experiment, the physiological environment of red blood cells was set as follows:

Change of pH value: adjust the pH value of red blood cell suspension to 5.6, 6.2, 6.8, 7.0, 7.2, 7.4, 7.6, 7.8, 8.0, 9.0, prepare one sample for each pH value.

Change of temperature: take the sample with pH 7.4, adjust the temperature of the microcell culture pool to change the temperature environment of the normal red blood cells through constant temperature circulating water supply, and set the temperature every 2°C in the range of 33-43°C continuous temperature rise.

Change of oxygen partial pressure: for the sample at pH 7.4 and 37°C, CO_2 gas is continuously introduced into the microcell culture cell for 30 min, and the oxygen partial pressure is changed to make Hb deoxidize. Two states of oxygenation (air > 95%, CO_2 < 5%) and deoxygenation (CO_2 > 95%, air < 5%) were set.

Change of osmotic pressure: for the sample at pH 7.4 and 37°C, add different amounts of water and 0.3 mol·L⁻¹ NaCl into the red blood cell culture medium to change the osmotic pressure. The set osmotic pressure is 438, 618, 711, 742, 798, 948, 1139 Pa.

Under the inverted microscope of AFM, the light beam of the tungsten-halogen stabilized current source (100 W) of the microscope passes through the aperture 1 with an adjustable aperture size, and then it is focused on the sample by the lens. The transmitted light of the sample collected by the objective lens passes through the intermediate relay lens and then enters the spectroscope through the detection diaphragm 2. The spectroscope consists of a reflection grating, which spreads the spectrum on the sensitive pixel of the CCD detector. The system software is compiled by the Boland Delphi5 software development system and runs under the multi-task operating system of Microsoft Windows 2000/98/NT. The virtual device driver technology is used to realize the computer control and data acquisition of CCD hardware system. The collected signal data is filtered/corrected by the computer.

During measurement, the sample is placed in a special sample tank, and the sample temperature is kept at 37°C. Adjust the diaphragm 1 so that the incident spot diameter is about 10 μL, and only one red blood cell is irradiated at a time. With 40× objective lens and 0.2 mm diaphragm 2 diameter, considering the intermediate relay lens (2×), the actual detection micro area diameter is 2.5 μm, then the internal wake-up absorbance of single red blood cell (normal diameter is about 7 μm) can be measured. Adjust the microscope, select a local area of a single red blood cell, set the appropriate CCD integration time, and measure. The light intensity $I_r(\gamma)$ of single red blood cells, the light intensity I_d of liquid transmission between adjacent cells and the dark output I_d generated by the dark current of CCD element were measured respectively.

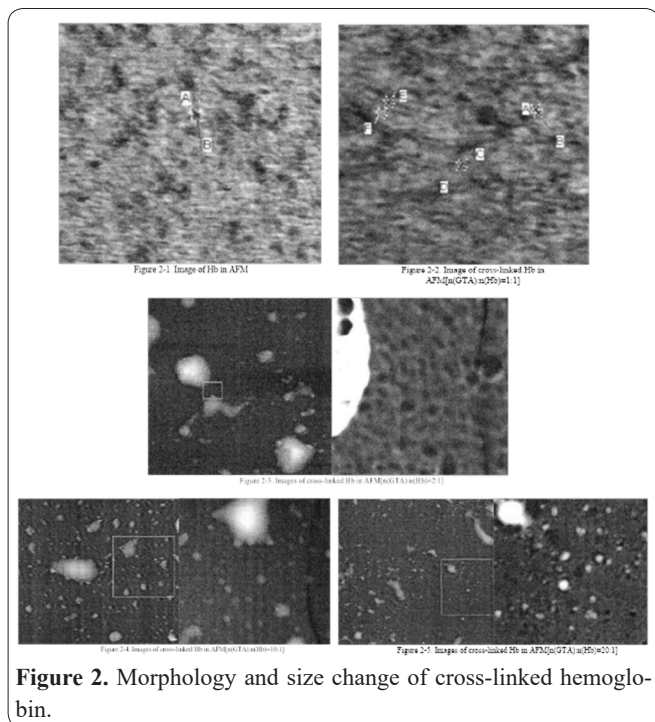


Figure 2. Morphology and size change of cross-linked hemoglobin.

Results

Morphology and size of cross-linked hemoglobin

Atomic force microscopy showed that the molecular size of un-cross-linked hemoglobin was about 6.64 nm (Figure 2-1), which was similar to the result of X-ray diffraction; it was the image with the molar ratio of glutaraldehyde to the hemoglobin of 1:1, and the particle size of un-cross-linked hemoglobin was similar to that of un-cross-linked hemoglobin, and the number of molecules with intermolecular cross-linking was less.

The molar ratios of glutaraldehyde to hemoglobin in Figures 2-3, 2-4 and 2-5 are 2:1, 10:1 and 20:1, respectively. When the molar ratio is 2:1, the particle size of cross-linked Hb is mostly kept at 20-30 nm; when the molar ratio is 10:1, the particle size below 30 nm accounts for the majority; when the molar ratio is 20:1, the cross-linked molecule diameter is about 30 nm; with the increase of the molar ratio, the cross-linked hemoglobin molecular size changes little, but the number of cross-linked molecules increases; the agglomeration of cross-linked molecules will make the particle size of some Hb molecules increase during the crosslinking process up to 80-100 nm.

With the increase of the molar ratio of glutaraldehyde to hemoglobin, the probability of binding between glutaraldehyde and hemoglobin molecules increases, and the number of Hb molecules participating in cross-linking increases. The size of the observed molecules increases with the aggregation of the cross-linked hemoglobin molecules. Because each glutaraldehyde molecule can intelligently cross-link two hemoglobin branches, the diameter of the cross-linked molecules will not increase indefinitely, which can be verified by the observation results of AFM.

Determination of hemoglobin and cross-linked hemoglobin peroxide activity

H₂O₂, 4-AAP and phenol (phenol) react in the ratio of 2:1:1 in Trinder color reaction. There was a charac-

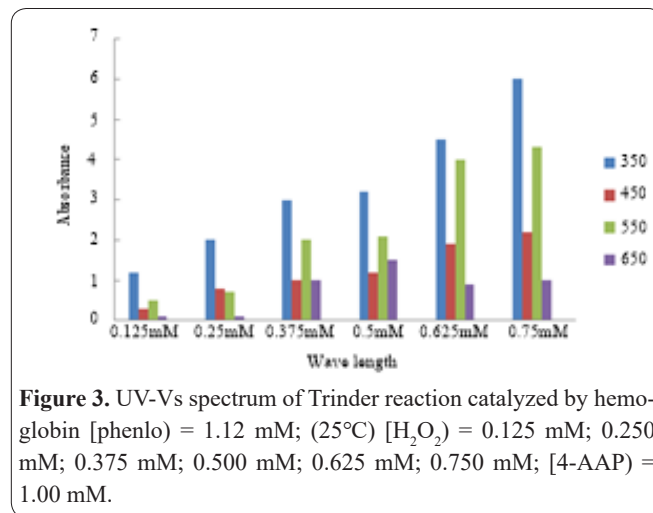


Figure 3. UV-Vs spectrum of Trinder reaction catalyzed by hemoglobin [phenol] = 1.12 mM; (25°C) [H₂O₂] = 0.125 mM; 0.250 mM; 0.375 mM; 0.500 mM; 0.625 mM; 0.750 mM; [4-AAP] = 1.00 mM.

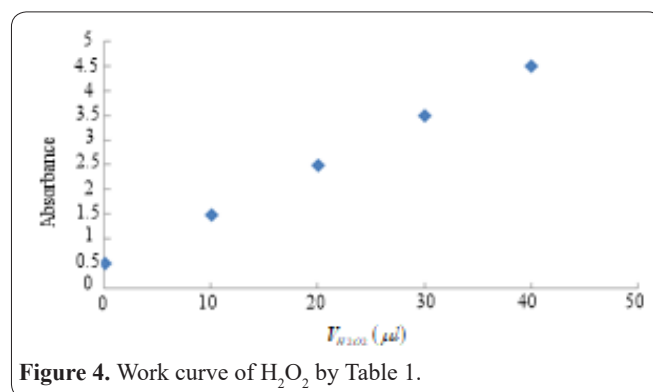


Figure 4. Work curve of H₂O₂ by Table 1.

teristic absorption peak at 505 nm. By measuring the absorbance of the substance at, the amount of waking substance generated can be calculated, thus the amount of H₂O₂ consumed can be obtained. During the reaction, excess of 4-AAP and phenol are allowed to fully carry out the reaction. When the absorbance of the generated wake-up is no longer increased, it can be considered that H₂O₂ completely reacts to generate wake-up substances. When the amount of H₂O₂ is not enough, the amount of wake-up products should be directly proportional to the amount of H₂O₂ added to the reaction system. The relationship can be determined by working images. Each scanning point is regarded as a time mode, and absorbance no longer increases with time. The absorbance at 505 nm and the corresponding amount of H₂O₂ added are as follows.

When the added H₂O₂ is not higher than 20 μL, the absorbance at 500.0 nm and the amount of H₂O₂ are basically in accordance with the formula: $y = 0.1395x - 0.2849$. The linear correlation coefficient $R = 0.9989$ can be obtained from $R^2 = 0.9976$, so there

Table 1. Relationship between the Absorption of product and the Amount of H₂O₂.

V(H ₂ O ₂) (μL)	Absorption
10	1.148
15	1.852
20	2.521
25	3.295
30	3.985
35	4.225
40	4.877

is a linear relationship between absorbance and H_2O_2 at a lower concentration. The reaction rate of H_2O_2 can be calculated from the change rate of absorption intensity. The molar absorption coefficient of the Quinone products absorbed by light is calculated as follows:

$$\delta = \frac{A}{bc} = \frac{0.650}{1 \times 0.125 \times 10^{-3}} = 5.20 \times 10^3 L \cdot mol^{-1} \cdot cm^{-1} \quad \{7\}$$

The effect of pH on the absorption spectrum of Hb

There are characteristic absorption peaks near 550 nm (α value) and 589 nm (β value) of hemoglobin solution in human erythrocytes. The height of absorption peak is not only related to the concentration of hemoglobin solution in erythrocytes but also related to the physical and chemical properties of hemoglobin (such as solubility, stability, oxidation state, etc.), and the position of absorption peak is related to the oxygen-carrying condition of hemoglobin.

When the pH value of the medium is low, the volume of the cell expands due to water absorption and the concentration of hemoglobin decreases accordingly. Therefore, the height of the characteristic absorption peaks at 550 nm and 589 nm is very low at low pH (see Table 2 and Figure 5). There is a significant difference between the two absorption peaks of hemoglobin with pH value between 5.6 and 7.2 and those with pH value equal to 7.4. However, there is no simple inverse relationship between the two absorption peak heights of hemoglobin and the change of RBC volume (i.e. the corresponding hemoglobin concentration change). In addition, when the pH value is equal to 5.6, the peaks of α and β shift from 550 nm-587 nm to 548 nm-585 nm when the pH value is equal to 7.4. This also shows that the decrease of hemoglobin absorption peak is the change of hemoglobin configuration caused by the decrease of hemoglobin concentration. First of all, the decrease of pH value of medium results in the decrease of RBC deformability, the change of hemoglobin configuration, the decrease of absorption peak height and the left shift of α and β peaks. When the pH value is equal to 7.6, the peaks of α and β do not shift to the left (Table 2), and the oxygen-carrying capacity of hemoglobin almost does not decline. The value of the increase of hemoglobin absorption peak caused by the increase of hemoglobin concentration in red blood cells exceeds the value of the decrease of absorption peak caused by the decrease of hemoglobin oxygen-carrying capacity. The-

refore, when the pH value is equal to 7.6, the absorption peak of hemoglobin is slightly higher than that when the pH value is equal to 7.4 (Table 2). When the pH value is equal to 7.8 and 8.0, the peaks of α and β shift 1-2 nm to the left (Table 2), and the oxygen-carrying capacity of hemoglobin decreases to some extent. The increase of absorption peak due to the increase of hemoglobin concentration is not enough to offset the decrease of oxygen-carrying capacity, so it is slightly lower than the absorption peak when pH value is equal to 7.4. From pH value equal to 7.4 to pH value equal to 8.0, there is no significant difference between the two absorption peaks of α and β of hemoglobin. When pH value equal to 9.0, the two absorption peaks drop sharply to 0.098 and 0.102 respectively, and there is a significant difference compared with pH value equal to 7.4 (see table 2). Due to the disturbance of the interaction between the cytoskeleton and lipid bilayer of the RBC membrane at high medium pH (e.g. 9.0), the vesiculation is caused. Some phospholipids on lipid bilayer contain some intracellular fluids (mainly hemoglobin solution), forming one and several microvesicles with a diameter of about 0.15-0.5 μm , which fall off from the mother cell, resulting in the decrease of hemoglobin concentration. In addition, with the increase of pH value of the medium, the intracellular hemoglobin interacts with the phospholipid cargo protein skeleton on the cell membrane and adheres to the inner side of the cell, which also reduces the hemoglobin concentration in the intracellular solution. However, considering that the volume of red blood cells at pH 9.0 is significantly lower than that at pH 7.4, the oxygen release coefficient, oxygen partial pressure and the binding capacity of hemoglobin and O_2 are reduced. Secondly, under the condition of low pH value, H^+ enters into the red blood cell and combines with the negatively

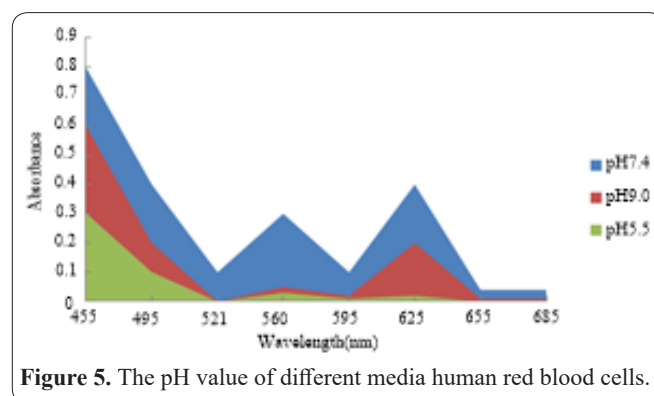


Figure 5. The pH value of different media human red blood cells.

Table 2. pH value of different media human red blood cells.

pH	α Peak		β Peak	
	Location(nm)	Absorbance	Location(nm)	Absorbance
5.6	550	0.055	585	0.078
6.2	550	0.025	585	0.069
6.8	550	0.038	585	0.086
7.0	550	0.061	585	0.095
7.2	548	0.071	589	0.158
7.4	550	0.125	587	0.198
7.6	550	0.156	589	0.201
7.8	549	0.125	589	0.185
8.0	549	0.108	589	0.156
9.0	548	0.098	585	0.102

charged hemoglobin molecule to shift the balance of $\text{Hb} + \text{H}^+ = \text{Hb}\cdot\text{H}^+$ to the right, reduce the zeta potential of hemoglobin and the stability of hemoglobin, cause the aggregation and precipitation of hemoglobin in the red blood cell, reduce the stability of hemoglobin, cause the aggregation and precipitation of hemoglobin in the red blood cell, and reduce the oxygen-carrying capacity of hemoglobin. Thirdly, when the pH value is equal to 7.4, the formation rate of metal hemoglobin (met Hb) is inhibited. When the pH value is greater than or less than 7.4, the formation rate of met Hb is accelerated, and the formation of oxygen and hemoglobin is also reduced.

When the pH value of the medium is greater than 7.4, on the one hand, the volume of red blood cells will shrink due to water loss, and the concentration of hemoglobin in the cells will increase, which will increase the absorption peak height of hemoglobin; on the other hand, with the increase of pH value, the deformability of red blood cells will decrease, and the oxygen-carrying capacity of hemoglobin will be smaller, so the concentration of hemoglobin should not be too small. Therefore, the main reason for the sharp decrease of the absorption peak height is obviously not the change of hemoglobin concentration, but the decrease of its oxygen-carrying capacity. It can be seen from Table 2 and Figure 5 that when the pH value is equal to 9.0, the α and β peaks move left to 548 nm and 585 nm respectively, which is equivalent to the absorption peak position when the pH value of the medium is equal to 7.2.

The function of hemoglobin and band 3 protein on the RBC membrane may be the reason why the absorption peak is higher than that at low pH value when pH value is equal to 9.0. In a neutral or acid medium (pH value is equal to 5.6-7.2), hemoglobin in RBC has a higher affinity with band 3 protein, and the lower the pH value of the medium, the greater the affinity, the closer the binding, and the adhesion to band 3 protein site on the surface of the bimolecular membrane, the more hemoglobin molecules there are. With the increase of pH value, the configuration of the band-3 protein hemoglobin complex began to change. The smaller the binding force between band-3 protein and hemoglobin molecule, the hemoglobin gradually separated from the band-3 protein. When the pH value is equal to 7.0, the binding force between hemoglobin and band 3 protein is very small; when the pH value is ≥ 8.0 , there is no binding force between hemoglobin and band 3 protein at all, so the hemoglobin molecules binding with band 3 protein are all separated. Therefore, when the pH value is equal to 9.0, the hemoglobin concentration in red blood cells is high when the swing arm is neutral or acidic so that the hemoglobin absorption peak when the pH value is equal to 9.0 is higher than the hemoglobin absorption peak when the pH value is less than 7.5.

In this experiment, the structure and function parameters of substances in red blood cells of athletes were measured without disturbance, in place and in real-time. In particular, the changes in hemoglobin molecular structure and oxygen-carrying capacity of athletes' red blood cells with medium pH values were reported for the first time. It not only provides an important experimental basis for biomedical research but also further proves that the new micro multi-channel spectrophotometry technology is a powerful tool to study the struc-

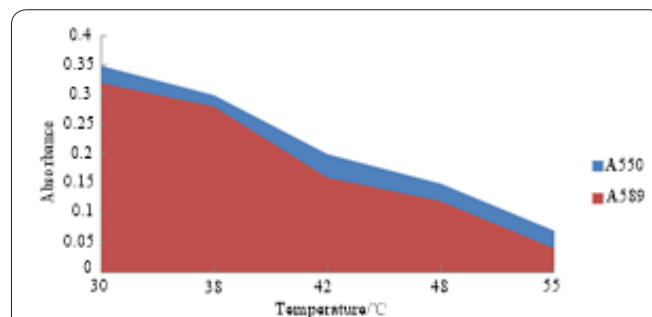


Figure 6. Absorbance variation with T.

ture and function of a single living cell.

The influence of temperature on the absorption spectrum of Hb

Figure 6 is the least square fitting result of Hb molecule A550 and A550 when the temperature changes continuously from 30°C to 55°C. With the increase of temperature, the peak height of the Hb absorption spectrum of normal red blood cells at 550 and 589 nm decreased gradually, the concentration of Hb in the cells decreased, the amount of Hb oxygen-binding decreased, and the function of oxygen delivery weakened. Therefore, there was a negative correlation between temperature and oxygen affinity. Figure 7 shows that at 43°C, 610 nm peak shape has obvious change, indicating that the molecular structure of Hb has changed.

The influence of oxygen partial pressure on the absorption spectrum of Hb

Figure 8 shows the absorption spectra of Hb in oxygenation and deoxygenation. The absorption spectrum curve of deoxygenation basically disappeared at 500nm, the amount of Hb oxygen binding was very low, and the oxygen content in cells was very little. This was because

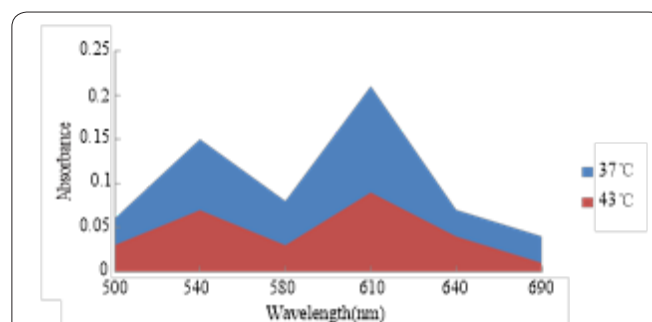


Figure 7. The absorption spectrum of intracellular Hb at different temperatures.

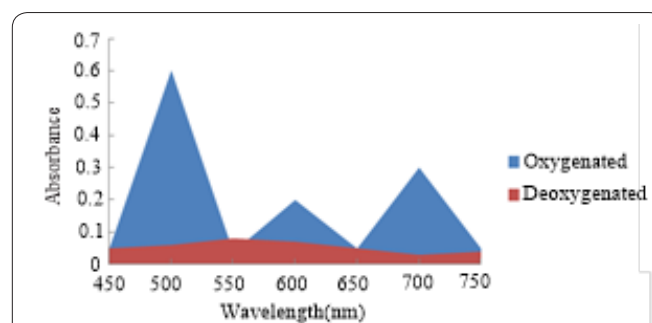


Figure 8. The absorption spectrum of intracellular Hb of oxygenated and deoxygenated states.

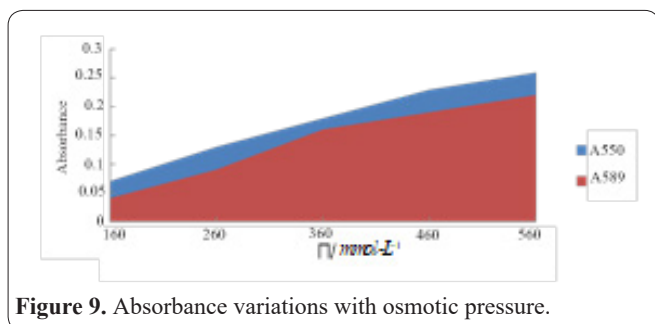


Figure 9. Absorbance variations with osmotic pressure.

the reaction of CO_2 and α -amino group in Hb formed a salt bond, which made Hb stable in the deoxygenation conformation, thus reducing the affinity for oxygen and the concentration of HbO_2 .

The Influence of osmotic pressure on the absorption spectrum of Hb

Figure 9 shows the fitting results of the least square method for the solubilized osmotic concentration (π) of HB molecule A550 and A589 with the change of osmotic pressure from 160 to 560 $\text{mmol}\cdot\text{L}^{-1}$. On the other hand, the concentration of Hb is one of the important factors that affect the viscosity of RBC. The internal viscosity increases exponentially with the increase of Hb concentration. The increase of the internal viscosity reduces the diffusion speed of Hb convection and O_2 , which leads to a decrease in the oxygen transport function of RBC. At the same time, a large amount of H^+ outside the membrane enters into the cell, which stabilizes the deoxidation conformation of the Hb molecule and reduces the affinity for oxygen by affecting the salt bond inside Hb molecule.

Discussion

Compared with an electron microscope, AFM has many advantages: for example, sample preparation is simple, sample conductivity can be suitable for the instrument; the operating environment is not limited, that is, it can be carried out in vacuum or the atmosphere, and the surface roughness value of the measured area can be calculated (13). Since the first atomic force microscope came out in the 1980s, its resolution and stability have been greatly improved, and its application range is wide (14). In addition, there are some other techniques to detect the hemoglobin in blood components (15, 16, 17, 18). Here, the morphology and size of hemoglobin and cross-linked hemoglobin were studied by AFM. The size of the uncross-linked hemoglobin was 6.64 nm, which was close to the reported value in the literature. When the molar ratio of glutaraldehyde to hemoglobin was less than 1, the hemoglobin was mainly intra-molecular cross-linked, and the cross-linked blood-red egg was not easy to occur when the molar ratio was greater than 1. In the process of cross-linking, the aggregation of cross-linked molecules will make the particle size of some Hb molecules reach about 80 nm. The results showed that the specific activity of cross-linked Hb decreased with the increase of the molar ratio of glutaraldehyde to Hb. However, when the molar ratio of glutaraldehyde to hemoglobin is 20:1, the specific activity of peroxidase of cross-linked hemoglobin can still reach more than 80% of that of uncross-linked hemoglobin; the cyclic

voltammogram of hemoglobin has good symmetry, which shows that the conversion between Fe^{3+} and Fe^{2+} is reversible, and the activity of hemoglobin may also be related to the conversion between Fe^{3+} and Fe^{2+} . At the same time, pH, temperature, oxygen partial pressure and osmotic pressure are all important factors affecting the molecular structure and function of Hb (19). Compared with pH values of 7.4, 9.0 and 5.5 respectively, when pH value is equal to 9.0, α and β peaks move left to 548 nm and 585 nm respectively, which is the same as the absorption peak position when pH value is equal to 7.2. The peak height, peak position and peak shape of hemoglobin absorption spectrum image at 550-589 nm have different processes change of degree. When the temperature changes continuously from 30°C to 55°C, the least square fitting results of the change of Hb molecules A550 and A589 show that with the increase of temperature, the peak height at 550 and 589 nm of Hb absorption spectrum of normal red blood cells gradually decreases, the concentration of Hb in cells decreases, the amount of HB oxygen-binding decreases, and the function of oxygen delivery weakens; the salt bond is formed by the reaction of CO_2 with an α -amino group in Hb, which makes Hb stable in the deoxygenation conformation, thus reducing the effect of The concentration of HbO_2 decreased with the decrease of oxygen affinity, and the peak of absorption spectrum disappeared at 500 nm. The amount of HbO_2 binding was very low, and the oxygen content in cells was very small. The results of the least-square fitting of the concentration of A550 and A589 of Hb molecules with the change of osmotic pressure (π) were from 160 to 560 $\text{mmol}\cdot\text{L}^{-1}$. With the increase in the concentration of Hb, the internal viscosity increased exponentially. The increase of the internal viscosity decreased the diffusion rate of Hb convection and O_2 . It can be seen that hemoglobin can measure various indexes of athletes' physical function and play an important role in athletes' physical function (20, 21). In addition to the subject matter, imaging have been widely used in many other subjects (22-40).

Atomic force microscopy (AFM) is an advanced technology for rapid and accurate qualitative, quantitative or local location analysis of cell components at the level of complete cells. It advances qualitative cytochemical methods to the research scope of digital local quantitative. AFM studies the size of cross-linked hemoglobin. When the molar ratio of glutaraldehyde to hemoglobin is less than 1, the hemoglobin is mainly intra-molecular cross-linked; when the molar ratio is greater than 2, with the increase of the molar ratio, the molecular particle size changes little, but the number of cross-linked molecules increases; during the process of crosslinking, the agglomeration of cross-linked molecules will make the particle size of some Hb molecules increase. The results of AFM showed that when the pH, temperature, oxygen partial pressure and osmotic pressure of RBC changed, the height, position and shape of the characteristic absorption peaks at 550 and 589 nm changed in varying degrees, which indicated that the change of physiological environment causes the change of molecular concentration and molecular structure of hemoglobin (Hb). The abnormal structure of oxygen delivery volume affects its oxygen affinity, which has important guiding significance for clinical diagnosis

and treatment. Therefore, the absorption spectrum curve of hemoglobin can be effectively observed by AFM to measure the physical function of athletes.

References

- Xue H, Zhang H. Research on airborne multi-functional rf integration system. *J Chin Acad Electron Info Technol* 2016; 11: 532-539.
- Xue Y, Zhou, L. Research on TCP enhancement in cognitive network based on cross-layer design. *J Chin Acad Electron Info Technol* 2016; 11: 208-213.
- Ding C, Leow MS, Magkos F. Oxytocin in metabolic homeostasis: implications for obesity and diabetes management. *Obesity Rev* 2019; 20(1): 22-40.
- Jiao X, Shi Z. The evaluation method of student performance in army simulation training system based on the grubbs calibration. *J Chin Acad Electron Info Technol* 2016; 11: 283-287.
- Kudryavtsev A. 3D Reconstruction in Scanning Electron Microscope: from image acquisition to dense point cloud (Doctoral dissertation, Bourgogne Franche-Comté).
- Zang W, Li Y, Wei G. Research on standards system and evaluation indicators for new type of smart cities. *J Chin Acad Electron Info Technol* 2018; 13: 1-7.
- Wang Q, Wang Z, Yao J. Conformance testing of new routing protocol in integrated space-terrestrial network. *J Chin Acad Electron Info Technol* 2018; 13: 72-80.
- Ge W. Secret sharing scheme based on Birkhoff interpolating polynomial. *J Chin Acad Electron Info Technol* 2018; 76: 170-173.
- Liu B, Su J. FrFT based adaptive interference suppression algorithm for time-varying wide-band interference. *J Chin Acad Electron Info Technol* 2016; 11: 319-325.
- Horak IR, Pasichnyk GV, Gerashchenko DS. cellular Plasticity as a driving force in cancer Progression: the regulatory role of adaptor Protein ruK/cin85. *The Ukrainian Biochemical Journal*. 2018; 90(3):102-3.
- Jiang H. Research on knowledge management system for defense science and technology intelligence in big data environment. *J Chin Acad Electron Info Technol* 2016; 11: 245-249.
- Chen H. A method of synthesizing range profile with a random lfm pulse signal. *J Chin Acad Electron Info Technol* 2016; 11: 636-641.
- Zhang H, Ma Z, Feng C. Comparison between sodar and wind tower data. *J Chin Acad Electron Info Technol* 2016; 11: 562-568.
- Cui J, Zhang Z. Analysis and evaluation of aircraft group with awacs cooperated combat on attacking area. *J Chin Acad Electron Info Technol* 2016; 11: 305-309.
- Jabin MA, Ahmed K, Rana MJ, Paul BK, Luo Y, Vigneswaran D. Titanium-coated dual-core D-shaped SPR-based PCF for hemoglobin sensing. *Plasmonics*. 2019 Dec 1; 14(6):1601-10.
- Ahmed K, Ahmed F, Roy S, Paul BK, Aktar MN, Vigneswaran D, Islam MS. Refractive index-based blood components sensing in terahertz spectrum. *IEEE Sensors Journal*. 2019 Jan 25; 19(9):3368-75.
- Ahmed K, Paul BK, Vasudevan B, Rashed AN, Maheswar R, Amiri IS, Yupapin P. Design of D-shaped elliptical core photonic crystal fiber for blood plasma cell sensing application. *Results in Physics*. 2019 Mar 1; 12:2021-5.
- Asaduzzaman S, Paul BK, Ahmed K, Bhuiyan T, Rahman SM. Highly sensitive SPR based PCF for biological substance sensing: design and analysis. In *Biophotonics: Photonic Solutions for Better Health Care VI* 2018 May 17 (Vol. 10685, p. 106851R). International Society for Optics and Photonics.
- Shao L, Huang C, Huang W. Study on optical interconnect module key position alignment offset post welding. *J Chin Acad Electron Info Technol* 2016; 11: 672-676.
- Yan N. Resisting power attacks scheme based on signed integer splitting form. *J Chin Acad Electron Info Technol* 2017; 12: 438-442.
- Zhang Y, Zhao X, Tu H. A queue management mechanism to improve 3d video transmission in WLAN. *J Chin Acad Electron Info Technol* 2017; 12: 246-250.
- Liang X, Shi W, Wang X, Qin J, Wang L, Wu X, et al. Brainstem schwannoma: A case report and review of clinical and imaging features. *Int J Radiat Res*. 2020; 18 (3) :605-610.
- ayeri H, Sattarzadeh Khameneh E, Zolghadri S, Kakaei S, Sardari D. Optimized production, quality control and biological assessment of 68-Ga-bleomycin as a possible PET imaging agent. *Int J Radiat Res*. 2020; 18 (2) :235-241.
- He X, Zheng J, Ren J, Zheng G, Liu L. Chest high-resolution computed tomography imaging findings of coronavirus disease 2019 (Covid-19) pneumonia. *Int J Radiat Res*. 2020; 18 (2) :343-349.
- Liu X, Shen C. Correlation of ultrasound perfusion imaging and angiogenesis of ovarian tumors. *Int J Radiat Res*. 2019; 17 (4) :559-567.
- Ahmadi N, Karimian A, Nasrabadi M, Rahmim A. Assessment of fetal and maternal radiation absorbed dose in 18F-FDG PET imaging. *Int J Radiat Res*. 2019; 17 (4) :651-657.
- Choi J, Rim C, Kim Y, Yang D. Cumulative radiation exposure dose of diagnostic imaging studies in breast cancer patients. *Int J Radiat Res*. 2019; 17 (2) :275-281.
- Salimi Y, Deevband M, Ghafarian P, Ay M. Uncertainties in effective dose estimation for CT transmission scan in total body PET-CT imaging with Auto mA3D tube current modulation. *Int J Radiat Res*. 2018; 16 (4) :465-472.
- Chen H, Huang H, Li G, Huang D, Huang S, Wang Z. Application of computed tomography and magnetic resonance imaging fusion images for delineating gross tumor volume in three-dimensional conformal radiotherapy of nasopharyngeal carcinoma. *Int J Radiat Res*. 2017; 15 (3) :251-257.
- Abtahi S, Jafari Khalilabadi R, Aftabi S. An investigation into the effect of magnetic resonance imaging (MRI) echo time spacing and number of echoes on the sensitivity and dose resolution of PAGATUG polymer-gel dosimeter. *Int J Radiat Res*. 2017; 15 (2) :185-196.
- Mahdavi S R, Jazayeri Gharehbagh E, Mofid B, Jafari A H, Nikoofar A R. Accuracy of the dose delivery in prostate cancer patients-using an electronic portal imaging device (EPID). *Int J Radiat Res*. 2017; 15 (1) :39-47.
- Heck K, Korkusuz Y, Happel C, Grünwald F, Korkusuz H. Percutaneous microwave ablation of thyroid nodules: efficacy evaluation with 99m Tc - pertechnetate and 99mTc-MIBI functional imaging. *Int J Radiat Res*. 2016; 14 (2) :91-98.
- Robotjazi M, Mahdavi S, Nikofar A, Bolouri B, Baghani H. Optimization of clinical target volume delineation using magnetic resonance spectroscopic imaging (MRSI) in 3D conformal radiotherapy of prostate cancer. *Int J Radiat Res*. 2014; 12 (4) :303-309.
- Jomehzadeh A, Shokrani P, Mohammadi M, Amouheidari A. A quality assurance program for an amorphous silicon electronic portal imaging device using in-house developed phantoms: a method development for dosimetry purposes. *Int J Radiat Res*. 2014; 12 (3) :257-264.
- Teimoori Sichani M, Amoui M, Akhlaghpour S, Hosntalab M. Quantitative SPECT and planar 32P bremsstrahlung imaging for dosimetry purpose –An experimental phantom study. *Int J Radiat Res*. 2014; 12 (2) :129-138.
- Salihin Yusoff M, Zakaria A. Determination of the optimum filter for qualitative and quantitative 99mTc myocardial SPECT imaging.

Int J Radiat Res. 2009; 6 (4) :173-182.

37. Jalilian A, Mirazizi F, Nazem H, Garousi J, Bolourinovin F, Sa-deghpour H. Preparation and quality control of radiolabeled streptokinase for Thrombosis imaging. Int J Radiat Res. 2009; 6 (4) :195-200.

38. Azadbakht B, Zahmatkesh M, Hadad K, Bagheri S. Verification of the PAGAT polymer gel dosimeter by photon beams using magnetic resonance imaging. Int J Radiat Res. 2008; 6 (2) :83-87.

39. Khosravi H, Sarkar S, Takavar A, Saghari M, Shahriari M. Planar and SPECT Monte Carlo acceleration using a variance reduction technique in I131 imaging. Int J Radiat Res. 2007; 4 (4) :175-182.

40. Jalilian AR, Fateh B, Ghergherehchi M, Karimian A, Matlloobi M. Preparation, distribution, stability and tumor imaging properties of [⁶²Zn] bleomycin complex in normal and tumor-bearing mice. Int J Radiat Res. 2003; 1 (1) :37-44.